Active fraction of ground cherry (*Physalis angulata* L.) calyces attenuates azoxymethane dextran sulfate sodium-induced colon carcinogenesis in mice

YANET OCAMPO[1*], DANEIVA CARO[1,2*], DAVID RIVERA[1], JENNY CASTRO[1,3], INDIRA PÁJARO[1,3], RUBÉN SALAS[1] and LUIS FRANCO[1]

[1]Biological Evaluation of Promising Substances Group, Faculty of Pharmaceutical Sciences, Universidad de Cartagena, Cartagena 130014, Colombia; [2]Dentistry Program, Universidad del Sinú-Elías Bechara Zainúm-Seccional Cartagena, Cartagena 130014, Colombia; [3]Faculty of Chemistry and Pharmacy, Universidad del Atlántico, Barranquilla 081007, Colombia

Received April 30, 2024; Accepted September 3, 2024

DOI: 10.3892/br.2024.1876

Abstract. *Physalis angulata* L., commonly known as wild tomato or ground cherry, is widely used in tropical and subtropical areas to treat health disorders including inflammation, hepatitis, dermatitis, cancer and diabetes. In Colombia, anti-cancer and anti-inflammatory activity are the most common ethnopharmacological applications of *P. angulata* calyces. *P. angulata* dichloromethane fraction (PADF) has significant anti-inflammatory activity. The present study assessed the pharmacological effect of PADF on colorectal cancer (CRC) using cancer and normal human cells and an azoxymethane (AOM)/dextran sulfate sodium (DSS) murine model. MTT and clonogenic assay, cell cycle and apoptosis analysis and mitochondrial membrane potential measurement were employed to evaluate *in vitro* activity of PADF. PADF selectively induced a cytotoxic effect against CRC cells via apoptosis and G2/M arrest. In the AOM/DSS model, treatment with PADF diminished tumor number and size, affected area and expression of proliferating cell nuclear antigen and promoted colon tissue repair. These effects might be related to the increased expression of p38 pro-apoptotic protein in addition to anti-inflammatory activity of PADF demonstrated by decreased levels of TNF-α, IL-6, and IL-1β. PADF may serve as a potential treatment for CRC. Further investigation is warranted to identify the bioactive components in PADF.

Correspondence to: Professor Luis Franco, Biological Evaluation of Promising Substances Group, Faculty of Pharmaceutical Sciences, Universidad de Cartagena, 29-11 Carrera 50, Cartagena 130014, Colombia
E-mail: lfrancoo@unicartagena.edu.co

*Contributed equally

Abbreviations: AOM, azoxymethane; CAC, colitis-associated cancer; CRC, colorectal cancer; DSS, dextran sulfate sodium; LPS, lipopolysaccharide; MAPK, mitogen-activated protein kinase; PADF, *Physalis angulata* dichloromethane fraction; PCNA, proliferating cell nuclear antigen

Key words: Physalis angulata L., AOM + DSS, CRC

Introduction

Physalis genus (Solanaceae family) comprises ~71 species distributed in America and Asian temperate regions (1,2). Plants belonging to this genus are recognized by the presence of calyces that cover the fruit protecting it from external damage (birds or insects and adverse climatic conditions) (2). The edible fruit and beneficial properties of teas prepared with different parts of the plants confer value within traditional medicine worldwide to treat inflammation, hepatitis, dermatitis, cancer and diabetes (2). Their biological activity is associated with the presence of withanolides (physalins, neophysalins, withaphysalins), labdane diterpenes, sucrose esters, flavonoids and ceramides (2-4). Among species of the genus *Physalis*, ground cherry (*P. angulata*) is used in Colombian folk medicine, as well in Asian and African countries, for its antimicrobial, antimalarial, anti-inflammatory, antinociceptive, anti-proliferative and immunomodulatory properties (4-7). It is effective against cervix, skin, lung, liver, gastric and colorectal cancer (CRC) (4,7). To the best of our knowledge, the biological properties of *P. angulata* calyces have been studied scarcely (2,4-6,8-10) despite their high levels of secondary metabolites for defense. In our previous research, fractionation of total ethanolic extract obtained from calyces yielded *P. angulata* dichloromethane fraction (PADF), which exhibited maintained or improved bioactivity particularly when evaluating its anti-inflammatory effect (6,8,9). PADF demonstrated a promising anti-inflammatory profile in experimental models [lipopolysaccharide (LPS)-stimulated RAW 264.7 macrophages, 12-O-tetradecanoylphorbol-13-acetate-induced acute ear edema and dextran sulfate sodium (DSS)-induced colitis] (6,9). The present study aimed to evaluate the effect of PADF on CRC cell lines and the azoxymethane (AOM)/DSS-induced colitis-associated cancer (CAC) mouse model. CRC is a serious public health problem that in 2020 caused worldwide nearly 1.9 million new cases and 915,880

deaths, being the third most common cancer diagnosed and the second leading cause of cancer death (11). Chronic inflammation, such as that found in inflammatory bowel disease, which includes ulcerative colitis and Crohn's disease, is considered one of the most common risk factors for the development of CRC, as it promotes tumor growth and development (12). CRC chemotherapy confronts serious challenges such as resistance, toxic reactions and side effects (13,14). Plants with biological activity may contain metabolites that facilitate development of novel therapy (14).

Materials and methods

Reagents and chemicals. AOM, crystal violet, Eagle's Minimal Essential Medium (EMEM), DMEM, hematoxylin-eosin (H&E), McCoy's 5A medium, protease inhibitor cocktail, and phenylmethylsulfonyl fluoride (PMSF) were purchased from Sigma-Aldrich (Merck KGaA). MTT was obtained from Calbiochem. DSS (36-50 kDa) was obtained from MP Biomedicals. Tissue Protein Extraction Reagent (TPER®) was obtained from Thermo Fisher Scientific, Inc. and fetal bovine serum (FBS) from Gibco (Thermo Fisher Scientific, Inc.). All solvents (ethanol, methanol, dichloromethane, hexane and DMSO) were reagent or HPLC grade.

Plant collection and preparation of PADF. P. angulata calyces were collected at Loma de Arena, Bolívar, Colombia. A sample of the whole plant was sent to Herbarium of the Universidad de Antioquia, Medellín, Colombia and authenticated according to a voucher previously deposited (no. HUA213028) (6). Clean and dried calyces were used for preparation of PADF according to the procedure described in a previous article (6) (Data S1).

Cell culture. Colorectal adenocarcinoma (HT-29 and Caco-2) and healthy colonic epithelial cells (CCD 841 CoN) were obtained from the American Type Culture Collection (ATCC) and maintained at 37˚C and 5% CO_2 in McCoy's 5A medium (HT-29) or EMEM (Caco-2 and CCD 841 CoN) supplemented with 10% FBS and 1.5 g/l sodium bicarbonate (Sigma-Aldrich; Merck KGaA).

MTT assay. HT-29, Caco-2 or CCD 847 CoN cells were seeded (5,000-15,000 cells/well) in 96-well plates (2D culture) or Perfecta3D® Hanging Drop Plate (3D culture; 3D Biomatrix) and incubated at 37˚C for 24 and 72 h, respectively, to allow attachment or spheroid formation, respectively. After that, cells were treated for 48 h at 37˚C with PADF (3.13, 6.25, 12.50 and 25.00 μg/ml), vehicle (MeOH), or Triton X-100 (1%) as a positive control. Cell viability was measured using MTT (0.25-5.00 mg/ml). After 4 h, formazan crystals were dissolved in DMSO, and the optical density (OD) at 550 nm was measured using a plate reader (Multiskan GO; Thermo Fisher Scientific, Inc.). Selective index (SI) was calculated as SI=IC_{50} of PADF in CCD 847 CoN cells/IC_{50} of the same compound in HT-29 or Caco-2 cells.

Clonogenic assay. The replicative capacity of HT-29 cells was confirmed as previously described (15,16). Cells (750 cells/well) were cultured into a 6-well plate at 37˚C for 6 h and treated with PADF (3.13, 6.25, 12.50 and 25.00 μg/ml) or vehicle for 48 h. Subsequently, the culture medium was refreshed and colonies were allowed to form for 7 days at 37˚C. Finally, colonies were fixed with 7:1 acetic acid-methanol at 24˚C for 30 min, stained with 0.5% crystal violet at 24˚C for 2 h, and counted manually using light stereomicroscope (EZ4 HD, Leica Microsystems GmbH; magnification, x10). A colony was considered to contain at least 50 cells.

Gap closure assay. HT-29 cells ($2x10^5$ cells/well) were grown with McCoy's 5A medium supplemented with 10% FBS (17,18), on μDish$^{35\ mm,high}$ plates (Ibidi) for 24 h (100% confluence). The insert was removed to generate a scratch in the monolayer, which was then treated with PADF (6.91 and 13.82 μg/ml) or vehicle. Images were captured at 24, 48 and 72 h with an inverted light microscope (Nikon Corporation; magnification x10). The open area in each image was measured using ImageJ 1.47v software (National Institutes of Health) and values were normalized to the open area at 0 h.

Cell cycle analysis. The impact of PADF on cell cycle distribution was determined by propidium iodide (PI) staining (cat. no. ab139418; Abcam) and analyzed using a FACS Aria III flow cytometer (BD Biosciences) and FlowJo X10.0.7 software (FlowJo LLC). HT-29 cells ($2x10^5$ cells/ml) were exposed to PADF (13.8, 18.0 and 27.6 μg/ml) for 24-48 h at 37˚C. Cells were harvested by trypsinization, fixed with 66% ethanol for 2 h at 4˚C, stained with PI and incubated with RNase A for 30 min at 37˚C in the dark. Doxorubicin (Doxo) was employed as a positive control.

Early and late apoptosis detection. HT-29 cells ($1\text{-}2x10^5$ cells/ml) were exposed to PADF (0, 13.8, 18.0 and 27.6 μg/ml) for 24-48 h at 37˚C. In the first assay, cells were stained with Annexin V-FITC (cat. no. BMS500FI-100; eBioscience) and analysis was performed using a flow cytometer (FACS Aria III, BD Biosciences) and the images were analyzed using FlowJo X10.0.7 software. For the second assay, DNA electrophoresis was used to detect DNA fragmentation using the apoptotic DNA ladder detection kit (cat. no. ab66093; Abcam) following the manufacturer's instructions.

Mitochondrial membrane potential ($\Delta\Psi m$). $\Delta\Psi m$ was monitored by JC-1 Mitochondrial Membrane Potential kit (Item No. 10009172; Cayman Chemical Company). Cells were incubated at 37˚C with JC-1 staining solution for 15 min and rinsed according to the manufacturer's instructions. Measurement was performed using a microplate fluorometer (Infinite 200 PRO, Tecan Group Ltd.) to quantify the fluorescence of J-aggregates (excitation 535 and emission 595 nm) and -monomers (excitation 485 and emission 585 nm).

Animals. Female Balb/c mice (mean weight, 19.41±0.13 g) were obtained from the Instituto Nacional de Salud (Bogotá, Colombia). Animals were housed in filtered-capped polycarbonate cages and kept in a controlled environment (19.48±0.10˚C, 68.63±1.15% humidity under a 12/12-h light/dark cycle) with access to food and water *ad libitum*. All experiments were designed and conducted following local and international regulations [European Union regulations (CEC council 86/809), EU Directive 2010/63/EU, protocols of the

Organisation for Economic Cooperation and Development] and approved by the Committee of Ethics in Research of the University of Cartagena (Project Approval Minute No. 81 from August 13, 2015).

AOM/DSS-induced CRC. The total experiment duration was 77 days (11 weeks). In brief, 5-6-week-old animals were randomized into control (vehicle), AOM + DSS and treatment groups (PADF 10 and 20 mg/kg, 6/group). Carcinogenesis was induced by intraperitoneal (IP) injection of AOM 10 mg/kg. One week later, animals received 2-4% DSS in drinking water for 7 days. To promote chronic inflammation-driven tumor progression, three DSS cycles at 2 weeks intervals (normal drinking water) were performed (19,20). Two doses of PADF (10 and 20 mg/kg, IP), selected according to previous study (6), and the acute toxicity test (Data S1), were administered for 3 weeks after the final DSS cycle, while control groups were treated with vehicle (saline). To check the safety of PADF, toxicity control groups administered PADF daily (10 and 20 mg/kg/day) without AOM or DSS. Body weight was monitored daily, while macroscopic parameters such as colon length and weight/length ratio and tumor progression (tumor number, size and load) were measured following sacrifice. Tumor load value was calculated as the sum of the diameters of all the tumors in each animal. A portion of the colon was rolled from the proximal to distal end. Samples of colonic tissue containing tumors and adjacent normal control tissue were also harvested for further analysis. The experiments had two sets of replications using 197 experimental animals in total. Sacrifice was performed by cervical dislocation following anesthesia by 2% inhaled sevoflurane. Animal death was verified by loss of heartbeat, reflexes and breathing. Humane endpoints were excessive weight loss (>4 g), diarrhea or hemorrhage. However, no animal was euthanized according to these endpoints.

Histology analysis. Colon samples were fixed with 4% buffered formalin for 30 days at 24˚C and embedded in paraffin; 5 μm sections were cut and stained with H&E and examined by two blinded researchers using light microscopy (cat. no. DM500, Leica Microsystems GmbH; magnification x10). Severity of mucosal inflammation, dysplasia and cancer were assessed. The epithelial damage and cellular infiltration were scored from 0-4 as previously described (21). Dysplastic proliferation was graded as low- or high-grade and scored considering the area of mucosal surface affected as absent (0), low- (1), medium- (2) or high-grade (3). Cancer was scored as absent (0), early invasive (1) or advanced (2).

Cell viability assay using conditioned media. RAW 264.7 macrophages (ATCC; cat. no. TIB-71) maintained in DMEM with 10% FBS at 37˚C and 5% CO_2, were cultured in 24-well plates (200,000 cells/well). After 48 h, macrophages were treated with 12.5 μg/ml PADF for 1 h and then stimulated for 6 h with LPS (1 μg/ml) or IL-4 (40 ng/ml) to induce an inflammatory M(LPS) or alternative M(IL-4) profile, respectively. Culture supernatant was collected and added to HT-29 cells seeded in 96-well plates (10,000 cells/well), which were incubated for 48 h at 37˚C. HT-29 cell viability was measured using the MTT method as aforementioned.

Protein expression analysis. Colonic tissue and HT-29 cells were homogenized using TPER® extraction reagent supplemented with protease inhibitor cocktail and PMFS for western blotting (Data S1) or cOmplete tablets Mini, EDTA-free (Roche Diagnostics GmbH) for ELISA. The extracted proteins were quantified with Bradford assay (Bio-Rad Laboratories, Inc.) using BSA as standard. The levels of IL-1β (cat. no. 88-7261-88), IL-6 (ref 88-7066-88; both Invitrogen), and TNF-α (cat no. 430204; BioLegend) in supernatant were measured using mouse ELISA kits following the manufacturer's instructions.

Statistical analysis. All data are presented as the mean ± SEM of ≥2 independent experiments. The half-maximal inhibitory concentration 50 (IC_{50}) was calculated using non-linear regression. Statistical analysis was performed by one-way ANOVA followed by Dunnett's multiple comparisons test. Statistical analyses were performed using GraphPad Prism 6 demo version (GraphPad Software, Inc.; Dotmatics). $P<0.05$ was considered to indicate a statistically significant difference.

Results

PADF extraction and chemical characterization. A total of 3.15 g PADF was obtained from 114 g dried calyces (2.76% yield) of *P. angulata*. Based on the information previously reported (6), four types of metabolites (withanolides, sucrose esters, phenolic compounds and flavonoids) were quantified for PADF chemical characterization. Only sucrose derivatives, most likely sucrose esters, were detected in significant amounts (Table SI; Data S1). There were low levels of withanolides and phenolic compounds and flavonoids were not detected.

Cytotoxic effect of PADF. Fig. 1A shows the inhibitory effect of PADF on the viability of colorectal adenocarcinoma cell lines. HT-29 and Caco-2 cells were notably sensitive to PADF, exhibiting IC_{50} values of 13.82±0.42 and 29.56±3.73 μg/ml, respectively. By contrast, normal colon epithelial cells (CCD 841 CoN) were not significantly affected by PADF at cytotoxic concentrations (12.5 μg/ml), displaying an IC_{50} of 44.80±1.77 μg/ml and selectivity index of 3.24 (HT-29) and 1.52 (Caco-2).

Due to the higher susceptibility of HT-29 cells, this cell line was selected to study the effect of PADF. Initially, its cytotoxic effect was tested at different exposure times; PADF exerted significant cytotoxicity at 6 h, which increased to a maximum at 48 h (Fig. S1A; Data S1). Due to the ability of HT-29 cells to form spheroids, 3D culture was also employed to mimic the cancer microenvironment better since it reflects physiological relevant cell-cell interactions (22-24). PADF showed a concentration-dependent effect, preserving the cytotoxic effect (IC_{50}=13.31±4.50 μg/ml; Fig. 1B) observed in the 2D model. Thus, this fraction demonstrates its ability to affect HT-29 cell viability in a tumor environment.

Effect of PADF on clonogenicity and migration of HT-29 cells. HT-29 cells formed multiple colonies after 7 days (Fig. 1C). This was inhibited by PADF treatment in a concentration-dependent manner. Similarly, PADF decreased gap closure of treated cells in comparison with control cells.

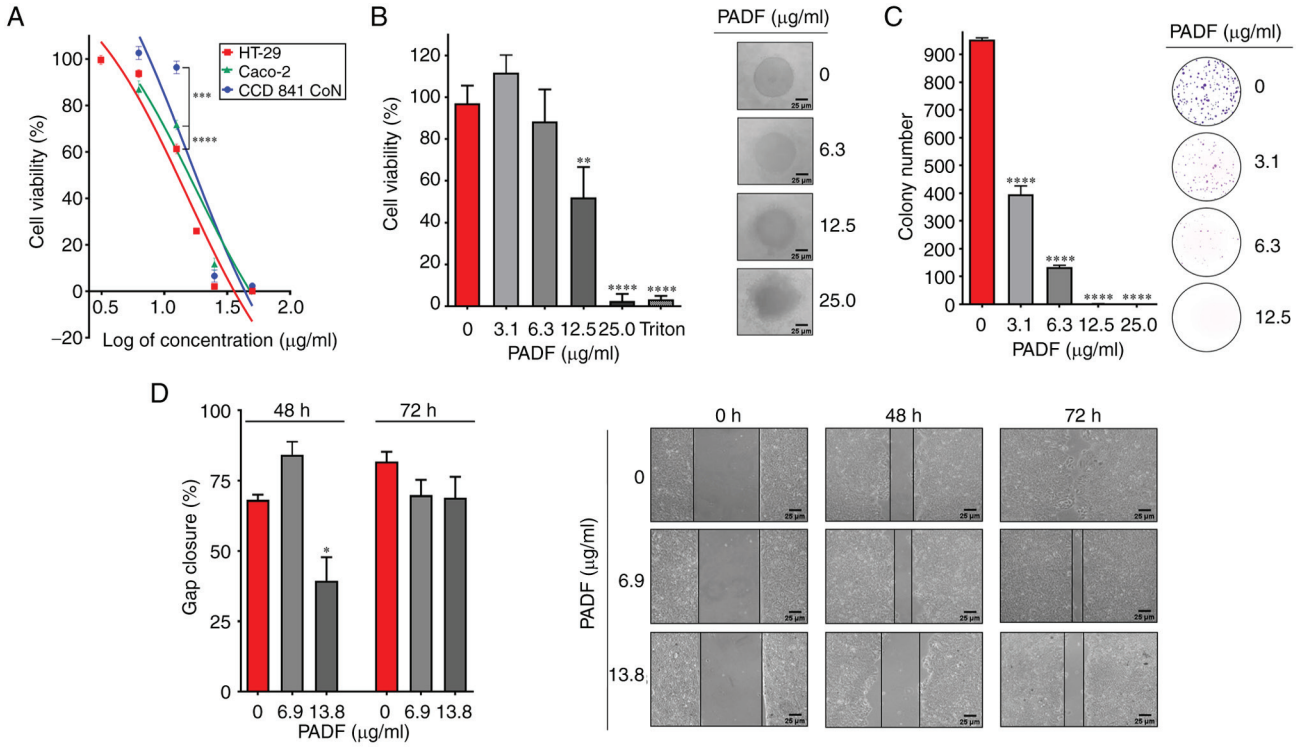

Figure 1. PADF affects viability and migration of colorectal cancer cells. (A) Effect of PADF on viability of malignant and normal epithelial colonic cells using MTT assay. (B) Cytotoxic activity of PADF against HT-29 cells spheroids (3D culture). (C) Effect of PADF on colony formation of HT-29 cells. (D) Assessment of PADF influence on HT-29 cell migration. Magnification, x10. n=12. **P<0.01, ***P<0.001 and ****P<0.0001 vs. untreated PADF, *Physalis angulata* dichloromethane fraction.

(Fig. 1D). Therefore, PADF affected not only the clonogenicity but also the migration of CRC cells.

Cell cycle and apoptosis analysis. Flow cytometry was employed to detect changes in cell cycle distribution. PADF induced cell cycle arrest in G2/M phase and significantly increased the proportion of sub-G1 cells, suggesting apoptosis induction (Fig. 2), which was corroborated by ΔΨM, Annexin V-staining and detection of DNA fragmentation. Annexin V-staining demonstrated that PADF induced a significant increase in the proportion of apoptotic cells (early and late), especially at the highest concentration (Fig. 3A). Consistently, this effect was accompanied by a significant reduction of ΔΨM, expressed as JC-1 fluorescence ratio, compared with control cells (Fig. 3B), as well as the degradation of DNA in PADF-treated HT-29 cells (Fig. 3C). To verify if apoptosis was associated with induction of oxidative stress by PADF, induction of reactive oxygen species (ROS) was measured; no change in ROS production was detected (Fig. S1B; Data S1).

In vivo assay. AOM-DSS produced a notable decrease in body weight on day 56; this loss of weight was significantly improved by the treatment with PADF at 10 mg/kg/day, while the higher dose (20 mg/kg/day) did not reverse this (Fig. 4A). Macroscopic assessment showed that 100% of animals in the AOM + DSS developed tumors (mean, 10.82±0.96 tumors in the middle and distal colon); by contrast, vehicle group showed no tumors (Fig. 4B). PADF (10 and 20 mg/kg/day) markedly reduced the total tumor load, specifically diminishing the number of tumors >1 mm in diameter. Furthermore, PADF significantly reduced the tumor size and tumor load by 35-85% (Fig. 4C-E). To assess the severity of the disease, colon weight/length ratio was measured; this was reduced in animals treated with PADF. Histological examination of colon sections stained with H&E of the AOM + DSS group confirmed large adenomas or adenocarcinomas inside the lumen and prominent extension of dysplasia (both high- and low grade) accompanied by slight inflammation of the epithelium and cellular infiltration (Fig. 5A and B). Conversely, PADF (10 and 20 mg/kg) promoted the recovery of tissue architecture by reducing tumor growth and dysplasia, thus lowering the histology score from 3.48±0.35 for AOM + DSS to 2.21±0.19 for PADF 20 mg/kg group (Fig. 5B).

During the study, the toxicity control group was monitored to verify that the administration of PADF did not alter the body weight of healthy mice; no signs of toxicity were detected at any dose (Table SII; Fig. S2; Data S1). Moreover, a detailed post-mortem analysis revealed no notable changes during necropsy and hematological analysis (Tables SII and SIII; Data S1). Likewise, PADF did not induce genotoxic effects, as established by the Ames test, micronucleus assay and comet assay (Fig. S2; Data S1), indicating the safety of PADF at effective dosage levels.

Protein expression analysis. PADF significantly reduced the levels of pro-inflammatory cytokines (TNF-α, IL-6, and IL-1β) in colon tissue compared with the AOM + DSS group (Fig. 5C). Based on the immunomodulatory effect on macrophages of PADF (6), it was assessed

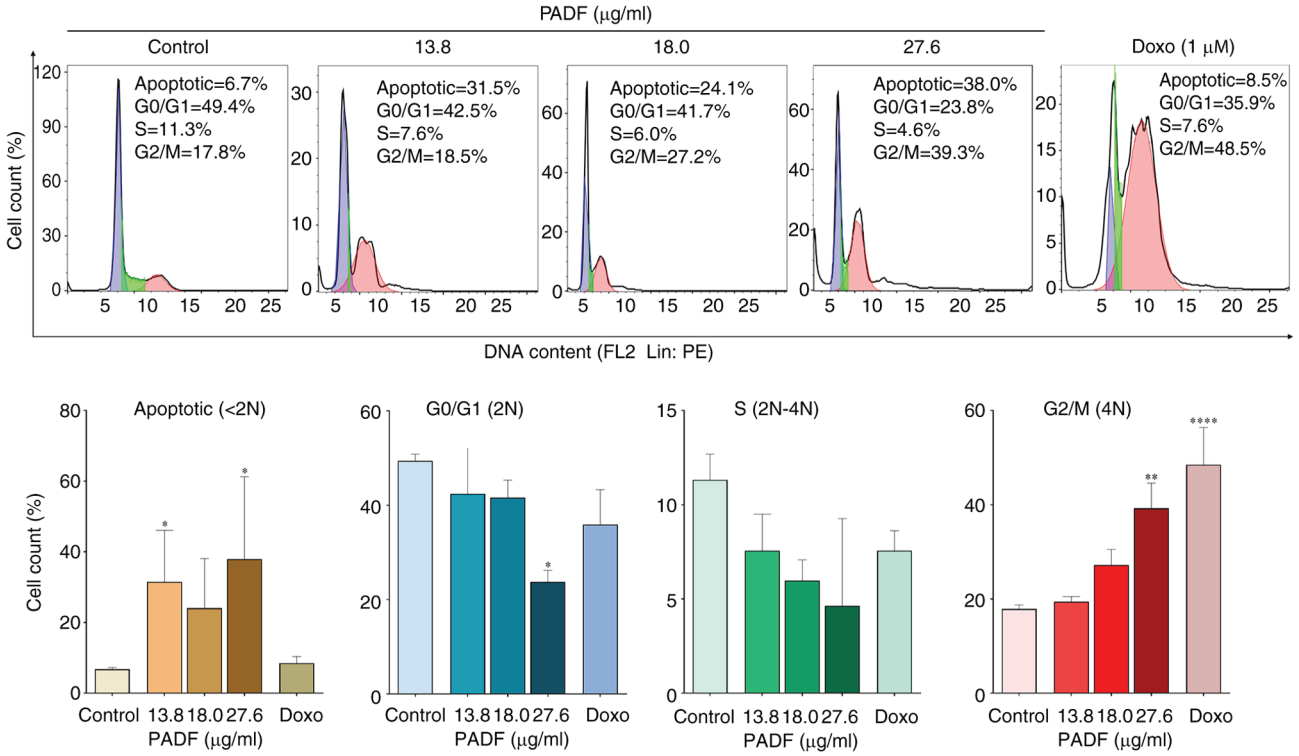

Figure 2. Cell cycle analysis of HT-29 cells following PADF treatment. n=12. *P<0.05, **P<0.01 and ****P<0.0001 vs. control. PADF, *Physalis angulata* dichloromethane fraction; Doxo, Doxorubicin.

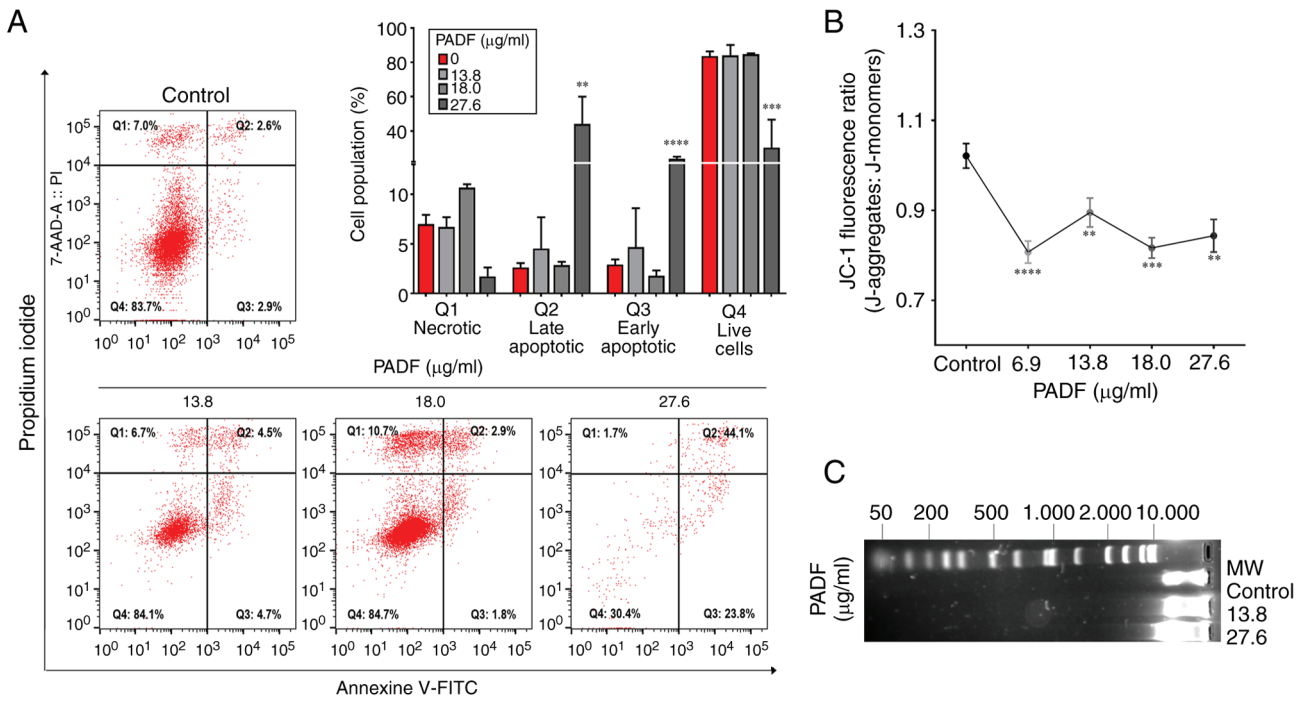

Figure 3. Apoptosis induction by PADF in HT-29 cell line. (A) Live, apoptotic and necrotic cell distribution. (B) JC-1 levels following treatment with PADF (6.91-27.64 μg/ml). (C) DNA fragmentation produced by PADF. n=12-32. **P<0.01, ***P<0.001 and ****P<0.0001 vs. control. PADF, *Physalis angulata* dichloromethane fraction; MW, molecular weight.

whether PADF inhibited viability of CRC cells treated with macrophage-conditioned media. Treatment with supernatants from LPS-stimulated macrophages decreases viability (Fig. 5D). By contrast, treatment with supernatants from IL-4-stimulated macrophages increased viability. However, when PADF (12.5 μg/ml) was administered, the viability of HT-29 cells was always significantly reduced, regardless of the conditional media.

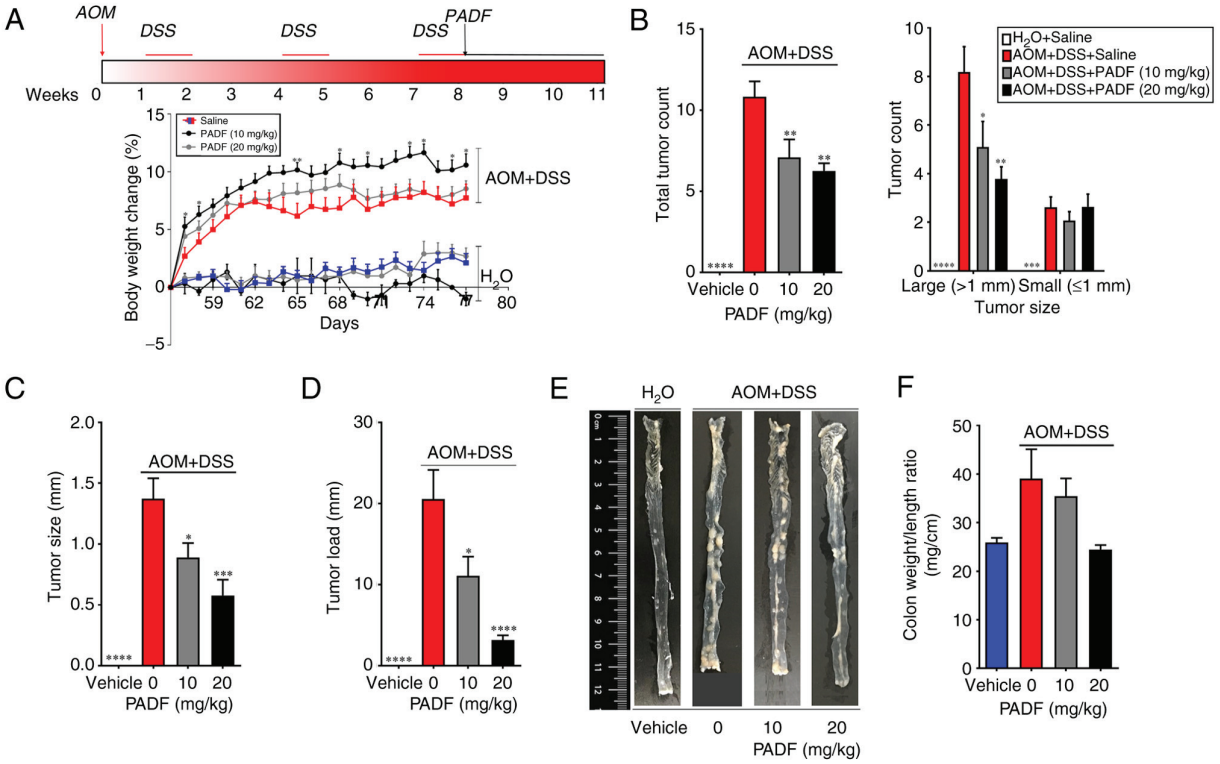

Figure 4. Therapeutic effect of PADF. (A) Experimental design and the body weight change. Tumor (B) number, (C) size and (D) load. (E) Representative macroscopic evaluation of colon tissue. (F) Colon weight/length ratio. n=12-32. *P<0.05, **P<0.01, ***P<0.001 and ****P<0.0001 vs. AOM + DSS. PADF, *Physalis angulata* dichloromethane fraction; AOM + DSS, azoxymethane + dextran sulfate sodium.

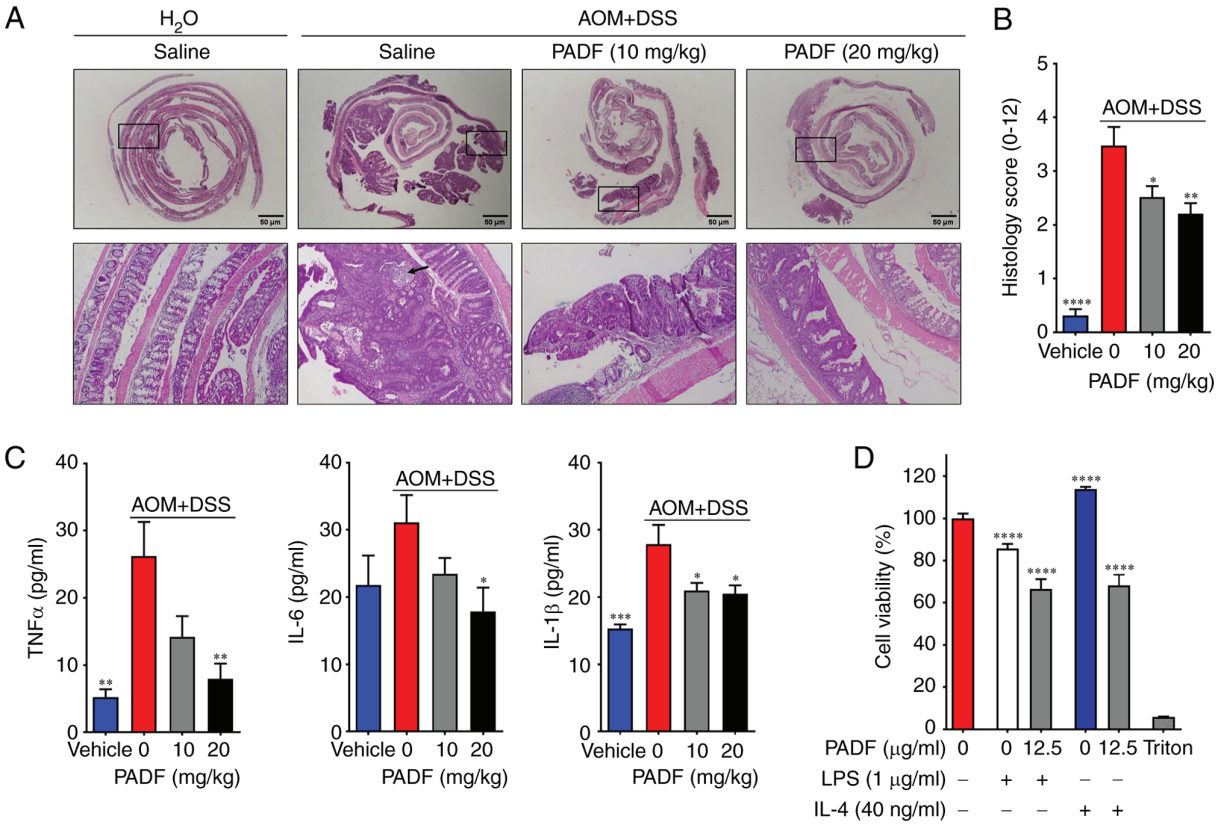

Figure 5. PADF improves microscopic damage induced by AOM + DSS in mice. (A) Representative histopathological examination by hematoxylin-eosin staining (magnification, x8 and x10; black arrow indicates crypt abscess). (B) Histological damage score. (C) Levels of pro-inflammatory cytokines in colonic tissue. (D) Viability of HT-29 cells treated with conditioning media of polarized M1 or M2 RAW 264.7 macrophages exposed to PADF. n=12-32. *P<0.05, **P<0.01, ***P<0.001 and ****P<0.0001 vs. AOM + DSS or untreated. PADF, *Physalis angulata* dichloromethane fraction; AOM + DSS, Azoxymethane + dextran sulfate sodium.

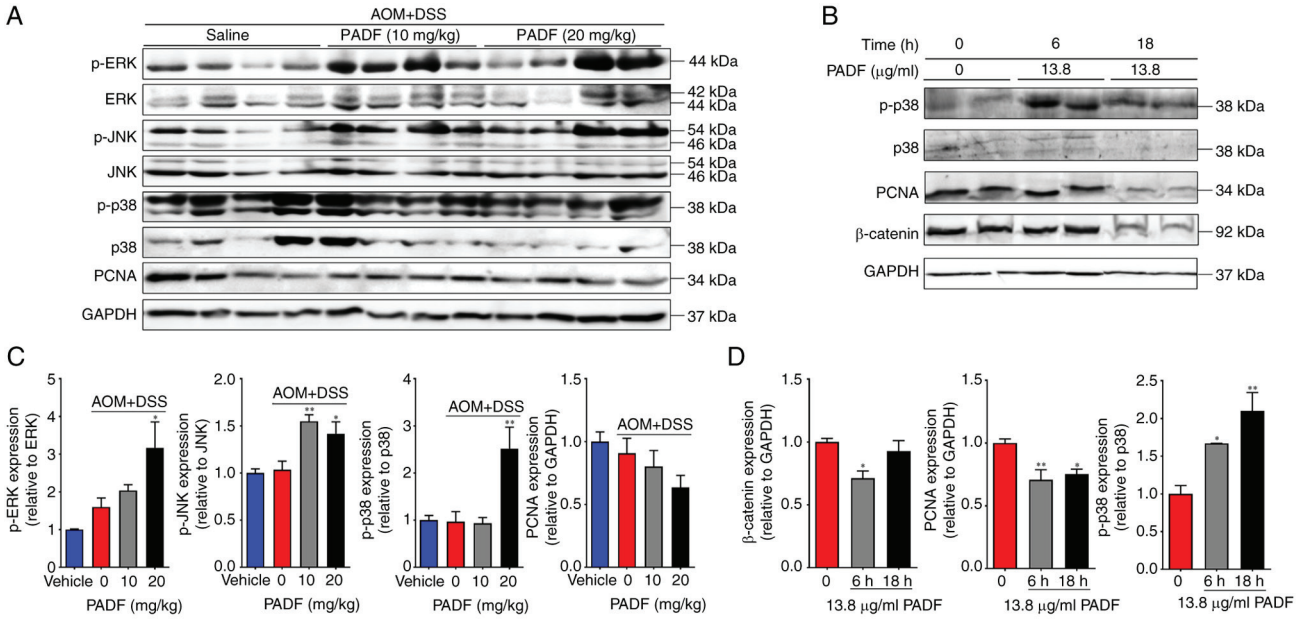

Figure 6. Expression of signaling proteins implicated in the progression of CRC tumors. (A) Representative western blot analysis of MAPKs (ERK, JNK, and p38) and PCNA in colonic samples. (B) Representative western blot analysis of p38 MAPK, PCNA and β-catenin in HT-29 cells. (C) Quantification of the protein expression of MAPKs (ERK, JNK. and p38) and PCNA in colonic samples. (D) Quantification of protein expression of p38 MAPK, PCNA and β-catenin in HT-29 cells n=4. *P<0.05 and **P<0.01 vs. AOM + DSS or untreated. PADF, *Physalis angulata* dichloromethane fraction; AOM + DSS, Azoxymethane + dextran sulfate sodium; PCNA, Proliferating cell nuclear antigen; p-, Phosphorylated.

Western blot analysis of colonic samples showed that PADF (10 and 20 mg/kg/day) significantly reduced the expression of proliferating cell nuclear antigen (PCNA) while enhancing that of phosphorylated MAPK in comparison with the AOM + DSS group (Fig. 6A and B). The decreased levels of PCNA and increased of p-p38 were confirmed in human CRC cells by western blotting (Fig. 6C and D).

Discussion

The present study demonstrated therapeutic potential of *P. angulata* calyces in CAC. Although the present study is not the first to identify the promising anti-tumor effect of derivatives from calyces of *Physalis* species (25), the present study combined *in vitro* and *in vivo* experiments to assess the effectiveness of PADF, as well as its mechanisms of action.

PADF chemical characterization revealed an enriched fraction in sucrose esters, metabolites detected in other *Physalis* species that exhibit anti-inflammatory properties (3,26,27). Although studies have reported sucrose esters with cytotoxic activity against human cancer cells in *Prunus tomentosa* (Rosaceae) and *Echium angustifolium* (Boraginaceae) (28-30), to the best of our knowledge, the present study is the first to report an anti-tumoral effect by a fraction enriched in sucrose esters in the *Physalis* genus.

The present results support the anticancer potential of PADF. PADF maintained cytotoxic activity on HT-29 cells in 2D (cell culture in a monolayer) and 3D models (spheroids). In addition, PADF demonstrated low cytotoxicity on CCD 841 CoN and another non-cancerous cell line (PCS-201-012; IC_{50}=30.71±1.92 μg/ml), reported in a previous study (8), further supporting its selective inhibitory activity against CRC cell lines. Although single-cell spheroids are a simple 3D approach to model CRC, the present results suggested that PADF may be effective in more complex experimental settings. The effectiveness as a cytotoxic agent was confirmed by colony formation assay (31), which demonstrated an inhibitory effect on the colony-forming ability at concentrations four times lower than the IC_{50}. Another technique used for screening antitumor drugs is the gap closure assay, which is used to evaluate the effects of selected drugs on cell migration, a feature of tumor metastasis that allows neoplastic cells to invade surrounding blood and lymphatic vessels and spread to other organs (31,32). PADF showed a potent inhibitory effect on HT-29 migration, making it a potentially useful alternative to be used in advanced stages of CRC where cells tend to invade other tissue.

To determine the mechanism of PADF underlying its cytotoxic activity on HT-29 cells, flow cytometry was employed. The results showed that PADF treatment induced apoptosis and G2/M arrest. G2/M checkpoint blocks the entry into mitosis when DNA is damaged to allow activation of repair mechanisms or the induction of programmed cell death (33). To confirm whether PADF triggered apoptosis, effects on early apoptosis were assessed by ΔΨM quantify J-aggregates and monomers, early/mid apoptosis assessing phosphatidylserine translocation by staining with Annexin-V, and late apoptosis by DNA fragmentation through electrophoresis (34). The present results confirmed that apoptosis occurred after PADF treatment of CRC cells.

Given the promising results *in vitro* as well as the strong anti-inflammatory activity observed previously (6), PADF was evaluated using a model of CAC, a disease resulting from the inflammation/dysplasia/carcinoma sequence where malignant cell proliferation, pro-inflammatory cytokines [IL-6, IL-1β and tumor necrosis factor (TNF)-α] and several signaling pathways (MAPK, NF-κB and Wnt/β-catenin) are hyperactivated (22). Animal models are key to identify carcinogens

and pathogenesis and progression of cancer and screen drug candidates during pre-clinical development. Despite its limitations, the combination of AOM and DSS as a model of CAC has popularity for its reproducibility, potency, low price and ease of use (35-39). The sustained release of pro-inflammatory cytokines and mediators (IL-1β, IL-6, TNF-α, nitric oxide and prostaglandin E2) can accelerate the process of colon carcinogenesis in both humans and mice (40-43). Therefore, these are important targets to assess when modeling CAC. PADF significantly decreased the levels of pro-inflammatory cytokines (TNF-α, IL-6 and IL-1β) in colon biopsies when compared with the AOM + DSS group. This anti-inflammatory effect, which promotes tissue recovery and mucosal regeneration, combined with the harmful effect against CRC cell lines, makes PADF an attractive alternative to treat CAC.

To assess the mechanism underlying with the beneficial effect of PADF, expression of PCNA and MAPKs (ERK, JNK, and p38) was determined as markers of abnormal cellular proliferation, inflammation, and stress response (44,45). PADF decreased PCNA phosphorylation and increased MAPK phosphorylation. As PCNA is involved with DNA synthesis and initiation of cell proliferation (40,43), this supported the inhibitory effect of PADF against malignant cells in CRC. However, increased MAPK phosphorylation by *P. angulata* appears contradictory since these proteins are traditionally associated with cancer pathogenesis (42,46,47). Nonetheless, activation of this pathway is dynamic during the inflammation/dysplasia/carcinoma sequence in the AOM-DSS model. For example, p-p38 is highly expressed during inflammation, but when carcinoma is established, expression of p-p38 decreases to normal levels. The elevated levels of p-p38 observed after administration of PADF in the high-grade dysplasia/carcinoma phase could be related to the induction of apoptosis in malignant cells, similar to that behavior observed with cisplatin, doxorubicin, and camptothecin (48,49), while protecting normal epithelial cells, a key role in the maintenance of epithelial homeostasis (50). Numerous naturally derived compounds (e.g., Phenethyl isothiocyanate, Evodiamine, Triptolide, Quercetin, and Honokiol) have been described as apoptotic inducers by increasing phosphorylation of JNK and ERK (49,51,52). The inhibition of PCNA and activation of p-p38 was confirmed using human CRC cells. β-catenin expression decreased, suggesting the inhibition of the Wnt signaling pathway, activation of which contributes to the initiation and progression of CRC (51).

In conclusion, PADF demonstrated potent cytotoxic, anti-tumor and anti-inflammatory activity in experimental models of CRC where viability of malignant cells was suppressed through apoptosis, cell cycle arrest, inhibition of cytokine expression and the modulation of key signaling pathways involving p38, PCNA, MAPKs and β-catenin. This bioactivity may be related to the high content of sucrose esters, metabolites with anti-inflammatory and antibacterial properties. Further investigations are needed to identify the compounds responsible for the activity.

Acknowledgements

The authors would like to thank Professor Josefina Zakzuk for support with flow cytometry and Ms. Jennifer Vazquez, Ms. Catherine Meza, and Ms. Laura Ospina for their assistance with the micronucleus assay (all Universidad de Cartagena, Cartagena, Colombia).

Funding

The present study was supported by Minciencias and Universidad de Cartagena (grant nos. 878-2015, 057-2018, and 025-2019).

Availability of data and materials

The data generated in the present study may be requested from the corresponding author.

Authors' contributions

LF conceived, designed and supervised the study and revised the manuscript. YO and RS designed the study. YO wrote the manuscript, constructed figures and supervised the study. LF, YO, IP, and RS confirm the authenticity of all the raw data. DC, DR, IP and JC analyzed data. DC performed experiments and wrote the manuscript. DR and JC performed experiments and revised the manuscript. IP and RS revised the manuscript. DR and IP constructed figures. All authors have read and approved the final manuscript.

Ethics approval and consent to participate

The animal study protocol was approved by Institutional Ethics Committee of the Universidad de Cartagena (protocol Minute No. 81 from August 13, 2015). All the experiments were designed and conducted following local and international regulations (European Union regulations (CEC council 86/809), EU Directive 2010/63/EU, protocols of the Organisation for Economic Cooperation and Development). In addition, tumor burden did not exceed the recommended dimensions according to University of Pennsylvania guidelines.

Patient consent for publication

Not applicable.

Competing interests

The authors declare that they have no competing interests.

References

1. *Physalis*-The Plant List. Version 1, 2010 [cited 2020 Feb 5]. Available from: http://www.theplantlist.org/browse/A/Solanaceae/Physalis/.
2. Mazova N, Popova V and Stoyanova A: Phytochemical composition and biological activity of *Physalis* spp.: A mini-review. Food Sci Appl Biotechnol 3: 56-70, 2020.
3. Zhang WN and Tong WY: Chemical constituents and biological activities of plants from the genus *Physalis*. Chem Biodivers 13: 48-65, 2016.
4. Rengifo-Salgado E and Vargas-Arana G: *Physalis angulata* L. (Bolsa Mullaca): A review of its traditional uses, chemistry and pharmacology. Bol Latinoam Caribe Plant Med Aromat 12: 431-445, 2013.

5. Cobaleda-Velasco M, Alanis-Bañuelos RE, Almaraz-Abarca N, Rojas-López M, González-Valdez LS, Ávila-Reyes JA and Rodrigo S: Phenolic profiles and antioxidant properties of *Physalis angulata* L. as quality indicators. J Pharm Pharmacogn Res 5: 114-128, 2017.
6. Rivera D, Ocampo Y and Franco LA: *Physalis angulata* calyces modulate macrophage polarization and alleviate chemically induced intestinal inflammation in mice. Biomedicines 8: 24, 2020.
7. Iwansyah AC, Luthfiyanti R, Ardiansyah RCE, Rahman N, Andriana Y and Hamid HA: Antidiabetic activity of *Physalis angulata* L. fruit juice on streptozotocin-induced diabetic rats. S Afr J Bot 145: 313-319, 2022.
8. Rivera DE, Ocampo YC, Castro JP, Caro D and Franco LA: Antibacterial activity of *Physalis angulata* L., Merremia umbellata L., and Cryptostegia grandiflora Roxb. Ex R.Br. -medicinal plants of the Colombian Northern Coast. Orient Pharm Exp Med 15: 95-102, 2015.
9. Rivera DE, Ocampo YC, Castro JP, Barrios L, Diaz F and Franco LA: A screening of plants used in Colombian traditional medicine revealed the anti-inflammatory potential of *Physalis angulata* calyces. Saudi J Biol Sci 26: 1758-1766, 2019.
10. Chouhan S and Guleria S: Anti-inflammatory activity of medicinal plants: Present status and future perspectives. In: Singh B (ed) Botanical Leads for Drug Discovery. Springer Singapore, pp67-92, 2020.
11. Sung H, Ferlay J, Siegel RL, Laversanne M, Soerjomataram I, Jemal A and Bray F: Global cancer statistics 2020: GLOBOCAN estimates of incidence and mortality worldwide for 36 cancers in 185 countries. CA Cancer J Clin 71: 209-249, 2021.
12. Nebbia M, Yassin NA and Spinelli A: Colorectal cancer in inflammatory bowel disease. Clin Colon Rectal Surg 33: 305-317, 2020.
13. Makin G: Principles of chemotherapy. Paediatr Child Heal 28: 183-188, 2018.
14. Safarzadeh E, Shotorbani SS and Baradaran B: Herbal medicine as inducers of apoptosis in cancer treatment. Adv Pharm Bull 4 (Suppl 1): S421-S427, 2014.
15. Franken NAP, Rodermond HM, Stap J, Haveman J and van Bree C: Clonogenic assay of cells in vitro. Nat Protoc 1: 2315-2319, 2006.
16. Yang X: Clonogenic assay to test cancer therapies. Bio Protocol 2: 1-3, 2012.
17. HT-29 | ATCC. Atcc.org, 2020. Available from: https://www.atcc.org/products/htb-38#detailed-product-information.
18. Weisser H, Göbel T, Melissa Krishnathas G, Kreiß M, Angioni C, Sürün D, Thomas D, Schmid T, Häfner AK and Kahnt AS: Knock-out of 5-lipoxygenase in overexpressing tumor cells-consequences on gene expression and cellular function. Cancer Gene Ther 30: 108-123, 2023.
19. Neufert C, Becker C and Neurath MF: An inducible mouse model of colon carcinogenesis for the analysis of sporadic and inflammation-driven tumor progression. Nat Protoc 2: 1998-2004, 2007.
20. Deng J, Zhao L, Yuan X, Li Y, Shi J, Zhang H, Zhao Y, Han L, Wang H, Yan Y, *et al*: Pre-administration of berberine exerts chemopreventive effects in AOM/DSS-induced colitis-associated carcinogenesis mice via modulating inflammation and intestinal microbiota. Nutrients 14: 726, 2022.
21. Obermeier F, Kojouharoff G, Hans W, Schölmerich J, Gross V and Falk W: Interferon-gamma (IFN-gamma)- and tumour necrosis factor (TNF)-induced nitric oxide as toxic effector molecule in chronic dextran sulphate sodium (DSS)-induced colitis in mice. Clin Exp Immunol 116: 238-245, 1999.
22. Kimlin LC, Casagrande G and Virador VM: In vitro three-dimensional (3D) models in cancer research: An update. Mol Carcinog 52: 167-182, 2013.
23. Atat O El, Farzaneh Z, Pourhamzeh M, Taki F, Abi-Habib R, Vosough M and El-Sibai M: 3D modeling in cancer studies. Hum Cell 35: 23-36, 2022.
24. Zibaei Z, Babaei E, Rezaie Nezhad Zamani A, Rahbarghazi R and Azeez HJ: Curcumin-enriched Gemini surfactant nanoparticles exhibited tumoricidal effects on human 3D spheroid HT-29 cells in vitro. Cancer Nanotechnol 12: 3, 2021.
25. Ballesteros-Vivas D, Alvarez-Rivera G, León C, Morantes SJ, Ibánez E, Parada-Alfonso F and Valdés A: Anti-proliferative bioactivity against HT-29 colon cancer cells of a withanolides-rich extract from golden berry (*Physalis* peruviana L.) calyx investigated by foodomics. J Funct Foods 63: 103567, 2019.
26. Ocampo YC, Caro DC, Rivera DE and Franco LA: Safety of sucrose esters from *Physalis* peruviana L. in a 28-day repeated-dose study in mice. Biomed Pharmacother 90: 850-862, 2017.
27. Zhang CR, Khan W, Bakht J and Nair MG: New antiinflammatory sucrose esters in the natural sticky coating of tomatillo (*Physalis* philadelphica), an important culinary fruit. Food Chem 196: 726-732, 2016.
28. Mora Vargas JA, Orduña Ortega J, Metzker G, Larrahondo JE and Boscolo M: Natural sucrose esters: Perspectives on the chemical and physiological use of an under investigated chemical class of compounds. Phytochemistry 177: 112433, 2020.
29. Wang Y, Wang Z, Sun Y, Zhu M, Jiang Y, Bai H, Yang B and Kuang H: Isovaleryl sucrose esters from Atractylodes japonica and their cytotoxic activity. Molecules 29: 3069. 2024.
30. Teng Y, Lan P, White LV and Banwell MG: The useful biological properties of sucrose esters: Opportunities for the development of new functional foods. Crit Rev Food Sci Nutr 64: 8018-8035, 2024.
31. Hatta MNA, Mohamad Hanif EAM, Chin SF, Low TY and Neoh HM: Parvimonas micra infection enhances proliferation, wound healing, and inflammation of a colorectal cancer cell line. Biosci Rep 43: BSR20230609, 2023.
32. Silva Nunes JP and Martins Dias AA: ImageJ macros for the user-friendly analysis of soft-agar and wound-healing assays. Biotechniques 62: 175-179, 2017.
33. Stark GR and Taylor WR: Analyzing the G2/M checkpoint. In: Checkpoint Controls and Cancer; Methods in Molecular Biology™. Vol. 280. Humana Press: Totowa, NJ, USA, pp51-82, 2004.
34. Chinnasamy S, Zameer F and Muthuchelian K: Molecular and biological mechanisms of apoptosis and its detection techniques. J Oncol Sci 6: 49-64, 2020.
35. Thaker AI, Shaker A, Suprada Rao M and Ciorba MA: Modeling colitis-associated cancer with azoxymethane (AOM) and dextran sulfate sodium (DSS). J Vis Exp: 4100, 2012.
36. De Robertis M and Signori E: Azoxymethane/dextran sodium sulfate (AOM/DSS) model of colorectal cancer. In: Čemažar M, Jesenko T and Lampreht Tratar U (eds) Mouse Models of Cancer. Methods in Molecular Biology. Vol. 2773. Humana, New York, NY, pp51-58, 2024.
37. Chen X, Ding Y, Yi Y, Chen Z, Fu J and Chang Y: Review of animal models of colorectal cancer in different carcinogenesis pathways. Dig Dis Sci 69: 1583-1592, 2024.
38. Lin R, Piao M, Song Y and Liu C: Quercetin suppresses AOM/DSS-induced colon carcinogenesis through its anti-inflammation effects in mice. J Immunol 2020: 9242601, 2020.
39. Lee YP, Chiu CC, Lin TJ, Hung SW, Huang WC, Chiu CF, Huang YT, Chen YH, Chen TH and Chuang HL: The germ-free mice monocolonization with Bacteroides fragilis improves azoxymethane/dextran sulfate sodium induced colitis-associated colorectal cancer. Immunopharmacol Immunotoxicol 41: 207-213, 2019.
40. De Robertis M, Massi E, Poeta M, Carotti S, Morini S, Cecchetelli L, Signori E and Fazio VM: The AOM/DSS murine model for the study of colon carcinogenesis: From pathways to diagnosis and therapy studies. J Carcinog 10: 9, 2011.
41. Giner E, Recio MC, Ríos JL, Cerdá-Nicolás JM and Giner RM: Chemopreventive effect of oleuropein in colitis-associated colorectal cancer in c57bl/6 mice. Mol Nutr Food Res 60: 242-255, 2016.
42. Takahashi M, Mutoh M, Kawamori T, Sugimura T and Wakabayashi K: Altered expression of beta-catenin, inducible nitric oxide synthase and cyclooxygenase-2 in azoxymethane-induced rat colon carcinogenesis. Carcinogenesis 21: 1319-1327, 2000.
43. Tang A, Li N, Li X, Yang H, Wang W, Zhang L, Li G, Xiong W, Ma J and Shen S: Dynamic activation of the key pathways: Linking colitis to colorectal cancer in a mouse model. Carcinogenesis 33: 1375-1383, 2012.
44. Ranganathan AC, Adam AP and Aguirre-Ghiso JA: Opposing roles of mitogenic and stress signaling pathways in the induction of cancer dormancy. Cell Cycle 5: 1799-1807, 2006.
45. Zhang L and Gu X: 4-hydroxysesamin protects rat with right ventricular failure due to pulmonary hypertension by inhibiting JNK/p38 MAPK signaling. Aging (Albany NY) 16: 8142-8154, 2024.
46. KRAS gene-Genetics Home Reference-NIH, 2020 [cited 2020 Mar 9]. Available from: https://ghr.nlm.nih.gov/gene/KRAS.

47. Vivona AA, Shpitz B, Medline A, Bruce WR, Hay K, Ward MA, Stern HS and Gallinger S: K-ras mutations in aberrant crypt foci, adenomas and adenocarcinomas during azoxymethane-induced colon carcinogenesis. Carcinogenesis 14: 1777-1781, 1993.
48. Bragado P, Armesilla A, Silva A and Porras A: Apoptosis by cisplatin requires p53 mediated p38alpha MAPK activation through ROS generation. Apoptosis 12: 1733-1742, 2007.
49. Cheung KL, Khor TO, Yu S and Kong ANT: PEITC induces G1 cell cycle arrest on HT-29 cells through the activation of p38 MAPK signaling pathway. AAPS J 10: 277-281, 2008.
50. Gupta J and Nebreda AR: Roles of p38α mitogen-activated protein kinase in mouse models of inflammatory diseases and cancer. FEBS J 282: 1841-1857, 2015.
51. Li W, Li C, Zheng H, Chen G and Hua B: Therapeutic targets of Traditional Chinese Medicine for colorectal cancer. J Tradit Chinese Med 36: 243-249, 2016.
52. Hu R, Kim BR, Chen C, Hebbar V and Kong ANT: The roles of JNK and apoptotic signaling pathways in PEITC-mediated responses in human HT-29 colon adenocarcinoma cells. Carcinogenesis 24: 1361-1367, 2003.